Quiescent and shear-induced crystallization of linear and branched polylactides

N. Najafi[1,2], M. C. Heuzey[1], P. J.Carreau[1], D. Therriault[2]

Research Center for High Performance Polymer and Composite Systems, CREPEC
1- Chemical Engineering Department, Polytechnique Montreal, Montreal, Quebec, Canada
2- Mechanical Engineering Department, Polytechnique Montreal, Montreal, Quebec, Canada

Abstract

The quiescent and shear-induced isothermal crystallization behavior of linear and long chain branched (LCB) polylactides (PLAs) was investigated at a temperature of 130°C. LCB-PLAs were produced by the reaction with a multi-functional chain extender, Joncryl©. In quiescent crystallization the presence of the LCB structure accelerated the nucleation process and reduced the induction time, depending on the level of branching. The impact of shear strain, and shear rate on crystallization was also examined. The shear-induced crystallization of the linear and LCB-PLAs was affected by both the total shear strain and shear rate. The crystallization kinetics of the LCB-PLAs was more affected by shear than that of the linear PLA. The crystalline morphology of the linear and LCB- PLAs under quiescent and step shear conditions was examined using a Linkam optical shearing system. An increase in the spherulite density was observed in the strained melt of both linear (33 %) and LCB-PLAs (15 %), in comparison with those of unstrained counterparts. Optical micrographs confirmed that the crystal nucleation was affected by the shear flow. . Long chain branching significantly promoted the nucleation density (6.7 times), although it diminished the crystal growth rate from 4.4 to 2.0 µm/min.

Keywords: polylactide, chain extender, long chain branching, shear-induced crystallization, induction time

1. Introduction

Polymer crystallization is a process involving partial arrangement of molecular chains initiated from nucleation and followed by subsequent crystalline growth (Ryan Anthony et al. 1999; Li et al. 2000; Kausch et al. 2005). The crystal formation and spherulitic structure in bulk polymers have been observed by atomic force (Li et al. 2000; Kausch et al. 2005) and polarized optical microscopy (Tsuji and Ikada 1996; Liu et al. 2012). Once the nucleation occurs, segments of a chain pull out of the amorphous phase, fold together and, sequentially, attach to the growth front, leading to the formation of an ordered structure called lamellae. The formed lamellae, then, arrange themselves into larger spheroidal entities named spherulites (Li et al. 2000; Kausch et al. 2005).

Polymeric materials generally form a semi-crystalline rather than fully crystalline structure (Jabbarzadeh and Tanner 2010), because chain ends act as defects. The mechanical and physical properties of semi-crystalline polymers have been found to strongly depend on the crystallization degree and type of morphology (Suryanegara et al. 2009; Han et al. 2013). The quality and level of crystallization, i.e. the nucleation density, size and shape of the crystallites, are affected by different factors including molecular weight, molecular structure, thermal history, cooling rate, presence of additives, and melt processing conditions (Hadinata et al. 2005; Yu et al. 2009; Jabbarzadeh and Tanner 2010; Najafi et al. 2013).

In most polymer processing operations such as extrusion, injection molding, fiber spinning, and film blowing, the polymeric chains are subjected to complex flow fields (elongation, shear, mixed flows) (Lellinger et al. 2003; Baert and Van Puyvelde 2006; Ma et al. 2013). Shearing the molten polymer during processing, indeed, plays a key role on crystallization and, therefore, on the final properties of the product (Lellinger et al. 2003; Yu et al. 2009; Jabbarzadeh and Tanner 2010; Ma et al. 2013). To provide a fundamental understanding of the crystallization phenomenon during

processing, it is required to separate the thermal and flow contributions. The global effect of flow on crystallization is known as flow-induced crystallization (FIC). To investigate FIC of polymers, steady shear and step-shear flows can be applied to the molten polymer (Wereta and Gogos 1971; Lellinger et al. 2003; Ma et al. 2013).

In the initial studies on flow-induced crystallization of molten polymers, Haas and Maxwell (1969) and Wereta and Gogos (1971) examined the structure evolution in continuous flow fields. Rheological parameters such as complex viscosity and dynamic moduli can also be monitored to study the kinetics of the crystallization process. For example, Yuryev and Wood-Adams (2010) considered the sensitivity of rheological properties to crystallinity to accurately determine the onset of crystallization. Once the crystals are nucleated and start growing from the melt state, the linear viscoelastic properties such as the complex viscosity, η^*, storage modulus, G', and loss modulus, G'', are found to increase since they are very sensitive to the structural changes occurring in the polymer (Madbouly and Ougizawa 2003). This stresses the impact of flow on the crystallization under steady shear, giving rise to a self-accelerating mechanism (Ma et al. 2013). Step-shear experiments were carried out by (Liedauer et al. 1993) where the sample was subjected to a step shear flow for a short time, and then, allowed to crystallize at rest. Two different strategies have been used in step shear flow studies: (i) applying shear in the molten state, followed by a quench to the final crystallization temperature (Madbouly and Ougizawa 2003; Jabbarzadeh and Tanner 2010), (ii) applying shear for short times at the crystallization temperature; then, after the cessation of flow induced nucleation is followed by crystal growth (Baert and Van Puyvelde 2006; Favaro et al. 2009; Ma et al. 2013).

Shear-induced crystallization has been investigated on high density polyethylene (HDPE) by Chen et al. (2007), on polybutene (PB) by Acierno et al. (2003), on polypropylene (PP) by Ma et al.

(2013), on polycaprolactone (PCL) by Lellinger et al. (2003), Madbouly and Ougizawa (2003), Acierno et al. (2006), on polytrimethylene terephthalate (PTT) by Favaro et al. (2009) and finally on polyethylene terephthalate (PET) by Ahn et al. (2002). In the vast majority of cases it was found that the shear flow mainly affected the crystal nucleation rate. Although shear-induced crystallization of linear polymers has been frequently investigated, only a few studies have examined the effect of long chain branching (LCB) on flow-induced crystallization (Heeley et al. 2006; Yu et al. 2009). It was reported that the presence of a small fraction of high molecular weight macromolecules significantly influences the shear-induced crystallization kinetics (Heeley et al. 2006; Yu et al. 2009).

Polylactic acid or polylactide (PLA) is a biodegradable, thermoplastic, aliphatic polyester synthesized from renewable resources such as corn, starch, and sugarcane (Drumright et al. 2000; Garlotta 2001; Najafi et al. 2012; Eslami and Kamal 2013). PLA can be synthesized either by direct condensation polymerization of lactic acid (Nagahata et al. 2007; Achmad et al. 2009; Wang et al. 2009) or ring opening polymerization of cyclic lactide (Kim et al. 1992). The synthesized polymer using these two methods is respectively called polylactic acid, with low molecular weight, and polylactide, which contains high molecular weight polymer chains (Lunt 1998). Stereo-chemically pure PLAs are categorized into *L*-lactide (PLLA) and *D*-lactide (PDLA) (Drumright et al. 2000). Depending on the *D*-lactide content, it can be semi-crystalline or totally amorphous (Drumright et al. 2000; Najafi et al. 2012). A synthesized PLA comprising less than 7 % *D*-lactide will be semi-crystalline, while the degree of crystallinity is enhanced with increasing *L*-lactide monomer purity (Drumright et al. 2000).

Polylactide is one of the most promising candidates from both economic and environmental perspectives to substitute some petroleum-based polymers such as polystyrene (PS), polyethylene

terephthalate (PET), and polyurethane (PU) (Garlotta 2001). A relatively low melt strength and non-strain hardening behavior of linear PLA is known to limit its applications in foaming, blow molding, and thermoforming (Liu et al. 2012; Wang et al. 2012b; Wang et al. 2012a; Eslami and Kamal 2013; Najafi et al. 2014). An efficient technique that has been used to improve the melt strength of linear polymers is the introduction of long chain branches into the polymer backbone (Najafi et al. 2012; Wang et al. 2012a; Eslami and Kamal 2013; Najafi et al. 2014).

In our earlier work (Najafi et al. 2012; Najafi et al. 2014), it was found that the incorporation of a multifunctional chain extender, Joncryl©, into PLA had a profound effect on the molecular weight and led to the formation of a long-chain branched (LCB) structure. The impact of the LCB structure on rheological properties and foaming behavior of PLA was discussed in details in our most recent study (Najafi et al. 2014). The aim of the present investigation is to determine the impact of the branched molecular structure and processing parameters on the isothermal quiescent and shear-induced crystallization kinetics, and morphology of PLA. To this end, LCB-PLAs were prepared in the presence of a multifunctional chain extender using two different PLA grades and different processing strategies. The experimental work is mostly based on rheometry. First, the quiescent crystallization behavior of linear and LCB-PLAs is examined. Then, the shear-induced crystallization kinetics and morphology of PLAs of different molecular structures are considered.

2. Experimental

2-1. Materials

The commercial grades of polylactide used in this study, PLA 3001D and PLA2003D, were purchased from NatureWorks LLC Co. (USA). They are semi-crystalline linear polyesters with *L*-lactide to *D*-lactide ratio of 98.5: 1.5 (Kramschuster and Turng 2009) and 95.75: 4.25 (Mujica-Garcia et al. 2014), respectively. As reported by the supplier, PLA 3001D, with a melt flow index

(MFI) of 22 g/10 min under a load of 2.16 kg at 210 °C, is less viscous than PLA 2003D with a MFI of 6 g/10 min in the same conditions. Joncryl® ADR-4368F was used as the chain extender (CE). It is a modified acrylic copolymer with multiple epoxy functions,which was supplied by BASF (Germany). Details on the reaction mechanisms of Joncryl with PLA can be found in Meng et al. (2012) whereas the effect of Joncryl on the rheological properties of PLA can be found in Najafi et al. (2012 and 2014).

2-2. Material Processing

Melt compounding of PLA with the chain extender (CE) was performed using a counter-rotating Brabender Plasti-Corder® internal mixer. Before compounding, the PLA granules were dried at 70 °C in a vacuum oven for 24 h. The dried PLA was then blended in the molten state with 0.4 and 0.7 wt% CE in the internal mixer at a set temperature of 185 °C. The mixing was conducted under a nitrogen atmosphere at a rotation speed of 100 rpm for 10 min, after which a relatively steady-state torque was established. Neat PLAs were dried, processed, and used as references in this study. To further examine the impact of CE and molecular topology, PLAs containing 0.4 wt% of CE were prepared using two different compounding strategies. In the first strategy (S1), PLA and 0.4 wt% of CE were directly mixed in the internal mixer under the aforementioned conditions. In the second strategy (S2), PLA was first compounded with 0.8 wt% of CE in the internal mixer for 10 min at conditions stated above. The resulting blend was dried in a vacuum oven (70 °C) for 24 h. Then, in the second run, it was mixed with the neat PLA at a weight ratio of 50:50 in the same conditions. The processed materials were placed in a vacuum oven (70 ºC) for 24h. To investigate the rheological properties, disk-shaped samples with 25 mm diameter and 1.5 mm thickness were prepared by compression molding. This process was conducted under a nitrogen atmosphere at 185

ºC and 20 MPa for 8 min, followed by a fast cooling to ambient temperature on a metal plate. The prepared samples were stored in a desiccator until used.

2-3. Characterization

The prepared disk-shaped samples were used to measure dynamic rheological properties. Small amplitude oscillatory shear (SAOS) experiments were conducted using a MCR-501 rotational rheometer (Anton Paar, Austria) with parallel plate flow geometry of 25 mm diameter and 1.1 mm gap size. The strain amplitude was set at 0.05, large enough to give a reliable signal while remaining in the linear viscoelastic regime prior to crystallization. The quiescent crystallization behavior was investigated at a frequency, ω, of 6.28 rad.s^{-1} and the results were then used as the reference point for the study of the shear-induced crystallization. To examine the effect of ω on the quiescent crystallization kinetics, measurements were also conducted at ω = 1 rad.s^{-1} for the neat PLA 3001D sample and for the 0.7 wt% CE formulation. The shear-induced isothermal crystallization studies followed the experimental protocol illustrated in Fig. 1: i) The disk-shaped sample was heated up to 190 ºC, above the polymer melting point (160 ºC), at a rate of 30 ºC/min under a nitrogen atmosphere. ii) The molten sample was held at this temperature for 10 min to remove the thermal history and obtain an isotropic melt. iii) The sample was cooled down to 180 ºC. iv) A constant shear rate ($\dot{\gamma}$) ranging from 0.1 to 1 s^{-1} was, then, applied to the melt for a time varying from 1 to 10 min prior to starting the test. v) The molten sample was cooled down to the crystallization temperature, T_c (120 or 130 ºC), at a rate of 30 ºC/min. vi) Time sweep tests were, thereafter, conducted at T_c and frequency, ω, of 6.28 rad.s^{-1} to monitor the the G' and η*.

In a previous study in our research group, Arias (2014) imposed a constant normal force throughout her rheological experiments to counterbalance the shrinkage of PLA during cooling and crystallization and improve the reproducibility of the tests. In the present work, the results

obtained using the normal force control were compared with those obtained without. No significant differences were observed and the measurements were therefore performed without imposing a normal force.

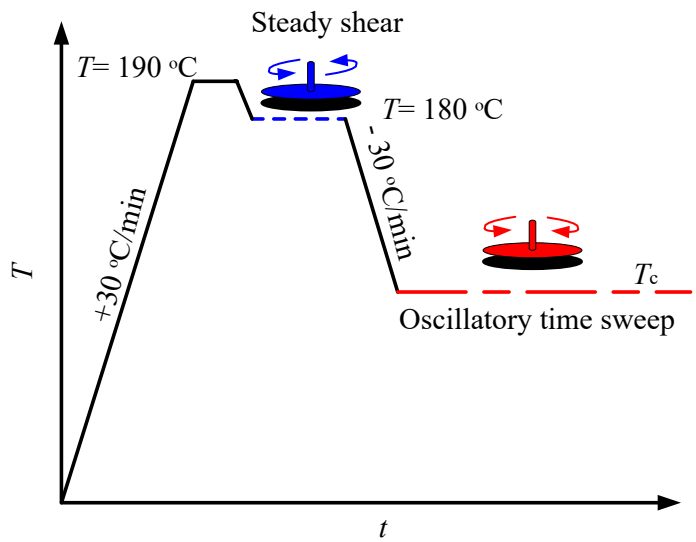

Fig. 1. Schematic representation of the thermal and pre-shearing treatments applied to the linear and LCB-PLAs before starting the isothermal crystallization test.

The morphology evolution of linear and LCB-PLA was monitored using a Linkam CSS450 (Surrey, UK) shearing hot stage in quiescent and shear flow conditions. This device operates with the same principle as a rotational rheometer with a parallel plate flow geometry. The Linkam system is able to impose shear on the melt although it cannot measure the melt viscosity (torque); hence, this instrument was strictly used for visualization purposes. To this end the sample was placed in the Linkam optical cell and heated up to 200 °C at 30 °C/min and kept for 10 min to eliminate the thermal history. The molten polymer was pressed between the two plates of the Linkam cell to achieve a gap of 200 μm. The sample was then cooled down to 180 °C and subjected to an imposed shear rate of 1 s^{-1} for 5 min. After stopping the shear flow, the temperature was reduced to the T_c (130 °C). In the absence of shear flow, the sample was directly cooled at the

same rate to the set temperature of 130 °C to observe crystallization. The pictures were then recorded by a CCD camera connected to a video recorder. Quantitative analysis of the digital images in terms of nucleation density and growth rate was carried out using appropriate software (ImageJ, NIH, USA)).

3. Results and Discussion

3-1. Crystallization in quiescent conditions

The quiescent crystallization behavior of linear and LCB-PLAs prepared using the two different strategies was investigated by rotational rheometer at *T* of 120 and 130 ºC.

Table 1. Initial value of the complex viscosity, $\eta^*_{t=0}$, of the linear and LCB-PLAs CE, at crystallization temperatures of (a) 120 and (b) 130 ºC. The frequency of the rheological test, ω, was set at 6.28 rad.s^{-1}.

Description			Sample Name	$\eta^*_{(t=0)}$ (kPa.s)	$\eta^*_{(t=0)}$ (kPa.s)
PLA grade	CE concentration (wt%)	Mixing strtategy		T=120 ºC	T=130 ºC
PLA2003D	0	S1	PLA2003-Neat	57.1 ± 1.4	33.9 ± 1.1
PLA 2003D	0.4	S1	PLA2003-0.4 J-S1	83.3 ± 2.7	60.1 ± 2.3
PLA 2003D	0.4	S2	PLA2003-0.4 J-S2	87.8 ± 2.5	68.5 ± 1.9
PLA 2003D	0.7	S1	PLA2003-0.7 J- S1	93.2 ± 4.6	73.6 ± 3.5
PLA3001D	0	S1	PLA 3001-Neat	42.7 ± 1.3	25.4 ± 1.3
PLA 3001D	0.4	S1	PLA3001-0.4 J-S1	59.2 ± 2.1	39.8 ± 1.9
PLA 3001D	0.4	S2	PLA3001-0.4 J-S2	65.8 ± 2.4	43.1 ± 2.1
PLA 3001D	0.7	S1	PLA 3001-0.7 J-S1	75.5 ± 3.5	55.1 ± 3.4

The evolution of η* with time is presented here. The initial values of η*of the linear and LCB-PLAs at crystallization temperatures of 120 and 130 ºC are presented in Table 1. The $\eta^*_{(t=0)}$ of the neat PLA 2003D is larger than that of the neat PLA 3001 D, due to its larger molecular weight. The incorporation of the chain extender into the neat PLAs, as shown here and discussed in our

previous work (Najafi et al. 2014), considerably increases its rheological response, depending on the CE content.

To ensure that the samples were free of crystals when starting the isothermal test at crystallization temperature, the initial values of the measured complex viscosity at t=0 ($\eta^*_{(t=0)}$) (Table 1) were compared with the values predicted by the Arrhenius equation at T_c.

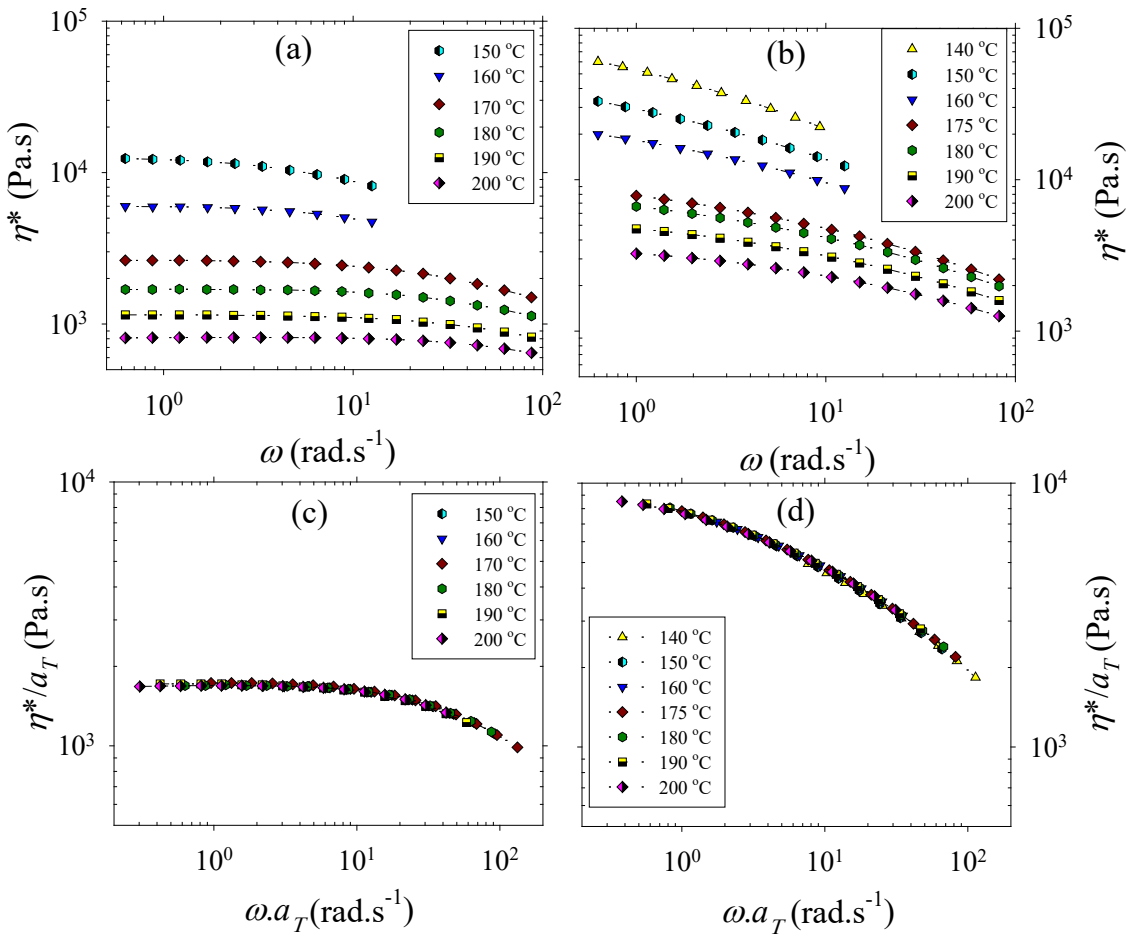

Fig. 2. The complex viscosity of (a) neat PLA 3001D, (b) PLA 3001D containing 0.4 wt% CE prepared using strategy S2, and the complex viscosity master curves of (c) neat PLA 3001D, (d) PLA 3001D containing 0.4 wt% CE prepared using strategy S2, at temperatures ranging from 140 to 200 °C.

To this end the SAOS data of two systems, the neat PLA 3001D, with low low crystallization rate, and the corresponding S2-compounded sample, with the highest crystallization rate, were obtained

at 200 °C and at lower temperatures down to 140 °C, following a cooling at 30 °C/min and during time periods short enough to avoid crystallization . Figs. 2a and b present the variations of the η^* as a function of ω for these systems at various temperatures, ranging from 140 to 200 °C. We note the very large viscosity increases as the temperature is decreased from 200 to 140 °C; also, as noted in Table 1 the viscosity of the PLA 3001D containing 0.4 wt% CE (Fig. 2b) is considerably larger than that of the neat PLA 3001D (Fig. 2a). The η^* data have been shifted using the shift factors obtained from the storage modulus and the master curves are plotted in Figs 2c and d. The calculated shift factors (a_T) over this broad range of temperatures (140-200 °C) are plotted in Fig. 3 (filled squares) to determine the flow activation energy (E_a).

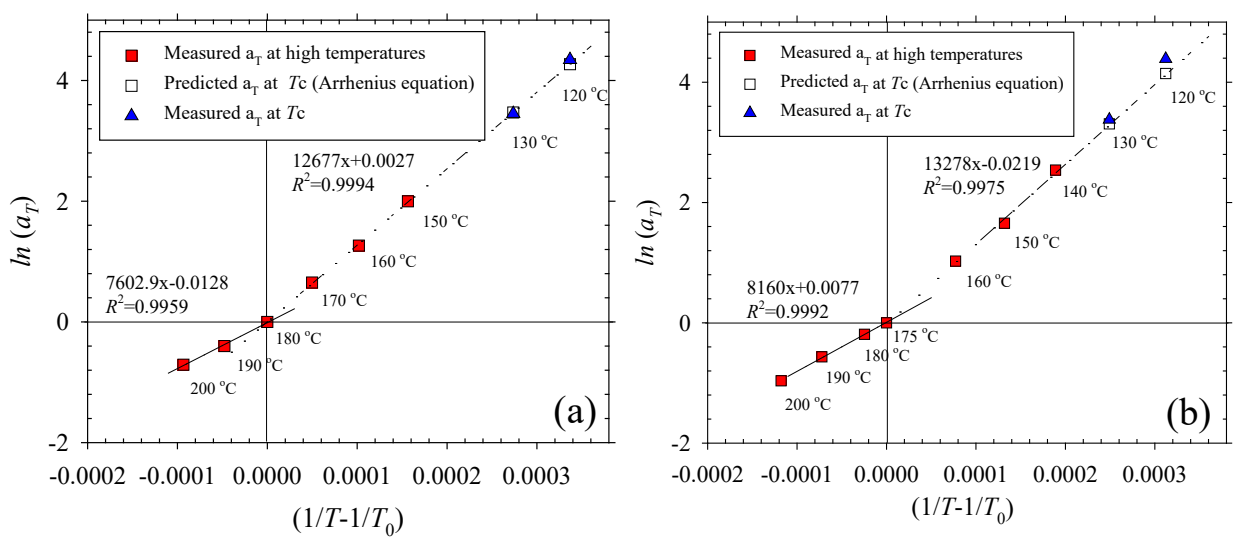

Fig. 3. Arrhenius plots of the shift factor as a function of the reciprocal (absolute) temperature for (a) Neat PLA 3001D, (b) PLA 3001D containing 0.4 wt% CE prepared using strategy S2, at temperatures from 120 to 200 °C.

A change of slope, related to E_a, is observed for the neat PLA at T = 180 °C and the S2-compounded sample at T = 175 °C (around T_g + 100 °C), indicating that the flow activation energy is temperature dependent over this broad temperature range. Therefore, a narrower range of data (the lower temperature region) was used to extrapolate the shift factors at T_c using the Arrhenius

law. The experimental shift factors at T_c (filled triangles) were obtained by horizontally shifting the initial value of the storage modulus ($G'_{t=0}$) along the frequency axis on the G' data obtained at the reference temperatures (180 °C for neat PLA, and 175 °C for the S2 sample). A comparison of the predicted (unfilled squares) with the measured (filled triangles) shift factors in Fig. 3a reveals that they are the same at T = 120 and 130 °C, confirming that the neat PLA contained no significant amount of crystals at the beginning of the isothermal crystallization test. Similarly, the measured shift factor of the S2-compounded sample at T = 130 °C (corresponding to η*=43.1 kPa.s) is quite close to the predicted one (η*=41.7 kPa.s). However, the measured complex viscosity at 120 °C (65.8 kPa.s) is higher than the predicted complex viscosity (59.7 kPa.s) from a_T (Fig. 3b), indicating the presence of a significant amoint of crystals at the beginning of the test at 120 °C.

In order to verify this possibility, tests with similar temperature cycling conditions were performed in differential scanning calorimetry (DSC). DSC results, (not shown here for brevity), showed that the crystallization onset (or induction) time for the neat PLA and S2-compounded sample was, respectively, 255 and 135 s at 130 °C. The onset time was reduced to 128 s in the case of the neat PLA and 65 s for the S2-compounded sample as the crystallization temperature was decreased to 120 °C. In the rheometer, once the temperature is lowered to T_c, the sample needs time to reach thermal equilibrium during which the viscoelastic properties rapidly increase and reach steady state values. Based on the rheological measurements, the minimum time to reach to steady state is estimated to be 100 s at T_c of 130 °C and 130 s at T_c of 120 °C. Considering that the time at 130 °C (100 s) is less than the onset time obtained from DSC measurements, it can be concluded that all the samples are free from crystals in these conditions. Similarly, the neat PLA is free of crystals when starting the SAOS isothermal test at T_c of 120 °C. Consequently, the measured complex

viscosity is the same as that predicted by the Arrhenius equation (Fig. 3). However, in the case of the S2-compounded sample, the time required to reach thermal equilibrium at 120 °C (130 s) is longer than its crystallization onset time (65 s from DSC). Hence, further crystallization studies were performed only at T_c = 130 °C.

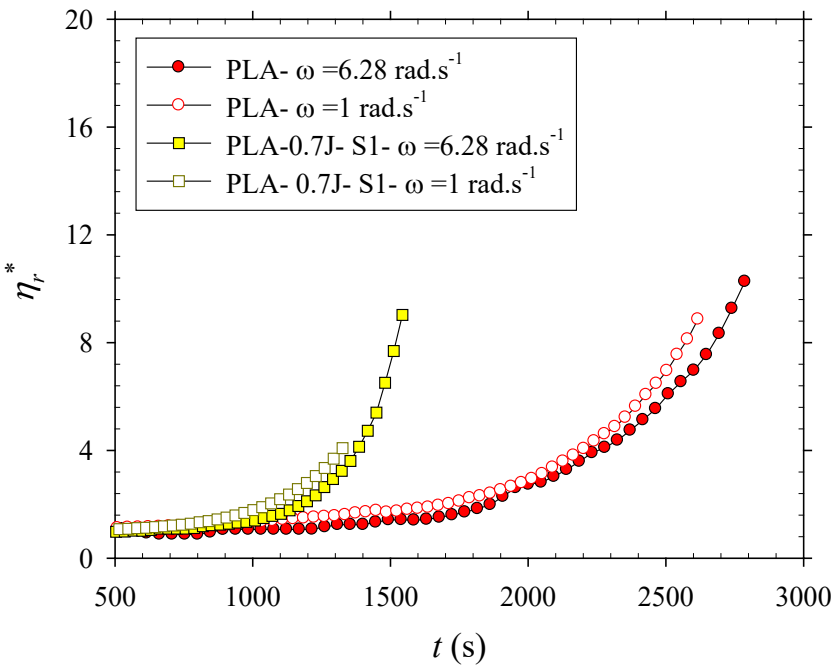

Fig. 4. Reduced complex viscosity, η_r^*, of the linear and LCB-PLAs (3001D) as a function of time at ω of 1 and 6.28 rad.s^{-1}. The crystallization temperature was set at 130 °C.

The effect of the applied frequency, ω, on the quiescent crystallization kinetics is illustrated in Fig. 4, which presents the reduced complex viscosity, $\eta_r^* = \eta^*_{(t)} / \eta^*_{(t=0)}$, of the linear and LCB-PLAs (PLA 3001D containing 0.7 wt% CE) as a function of time at frequencies of 1 and 6.28 rad.s^{-1} and T_c of 130 °C. The η_r^* value starts to slowly increase at the early stage of the test, and then increases rapidly. The substantial increase in η_r^* with time is attributed to the growth of the nucleated crystals, leading to continuous increase in the crystalline fraction that may act as cross-

links (Madbouly and Ougizawa 2003). Due to transducer overload near the end of the crystallization process, the later data are not reliable and not reported. The results shown in Fig. 4 indicate that the onset of crystallization is marginally affected by the frequency although the crystallization kinetics seem to increase slightly with decreasing the frequency. This may result from the decreased elasticity and stiffness of the polymer chains, facilitating the chain–folding process (Hu 2001). Considering that the effect of ω on crystallization is marginal, further studies were conducted at ω = 6.28 rad.s^{-1}.

The η_r^* evolution of both grades of PLA, PLA 2003D and PLA 3001D, containing various quantities of CE is presented as a function of time at ω of 6.28 rad.s^{-1} and T of 130 ^{o}C in Figs. 5a and b, respectively. The neat PLAs have a linear structure with virtually no branching. The addition of 0.4 wt% CE to the neat PLA using strategy S1 results in the formation of a LCB structure. In strategy S2, increased CE content (in the first run) favored the formation of a more developed LCB structure in the compounded sample, as compared with that prepared using S1 (Najafi et al. 2014).

The induction time of crystallization, t_{in}, is an important characteristic of the kinetics of crystallization. The standardized residuals technique, r_i, (Eq. 1) was used to determine the induction time of PLA crystallization:

$$r_i = \frac{e_i}{\sqrt{\sigma^2}} = \frac{e_i}{\sqrt{\frac{1}{n-1}\sum_{i=1}^{n}(e_i - e)^2}} \tag{1}$$

where, e_{i} is the real residual and the divider is the standard deviation of the residuals. This method has been reported to effectively define the induction time of PLA crystal formation (Yuryev and Wood-Adams 2010). In the present study, the residuals were determined as the differences

between the measured complex viscosity and the initial value of the complex viscosity ($\eta^*_{t=0}$). The standardized residuals for the linear and LCB-PLAs (PLA 2003D and 3001D) at 130 ºC are presented in Figs. 6a-d. Their initial values are close to zero for some time, after which a sharp rise is observed. To determine the induction time of crystallization, a straight horizontal line was drawn at a standardized residual value of 0.1. The time at which the curves cross this straight line is arbitrarily defined as the induction time.

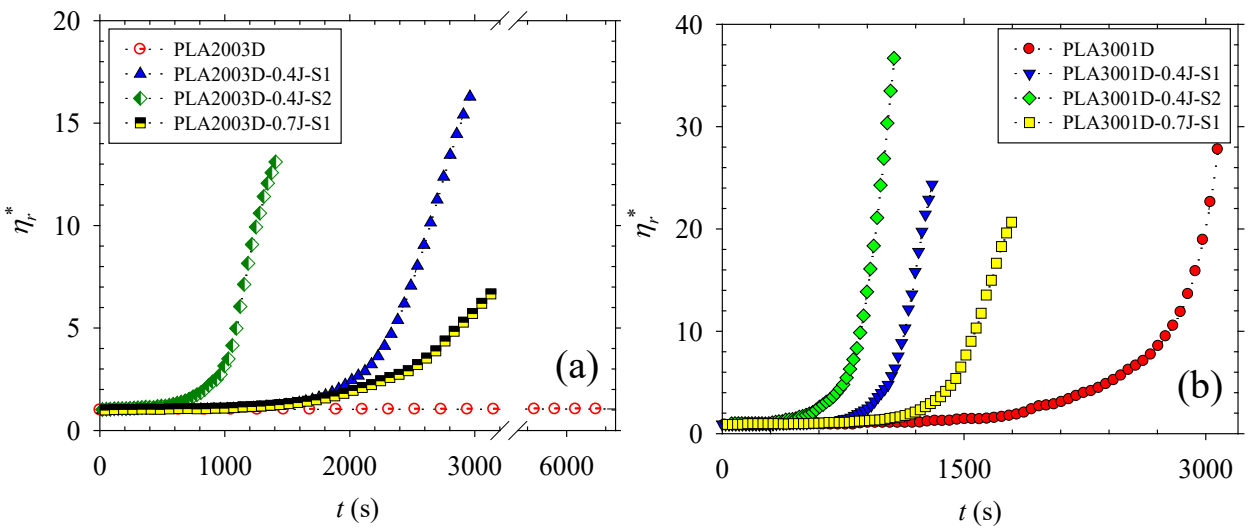

Fig. 5. Normalized complex viscosity, η_r^*, of (a) PLA 2003D, (b) PLA 3001D with various contents of CE prepared using different strategies, as a function of time at 130 ºC.

The induction time, t_{in}, values for the linear and LCB-PLAs prepared using both grades of PLA at 130 ºC are reported in Table 2. The experimental variability on t_{in} is less than 8 % in this work. For the neat PLAs, shown in Fig. 6a and reported in Table 2, the onset of crystallization occurs after a long annealing time (t_{in} of PLA 2003D is not observed and that of PLA 3001D is 1890 s), suggesting that the isothermal crystallization of PLA is quite slow (Arias et al. 2013). In comparison with PLA 2003D, PLA 3001D exhibits a shorter induction time due to its lower *D*-content, lower M_W, and higher crystallization ability.

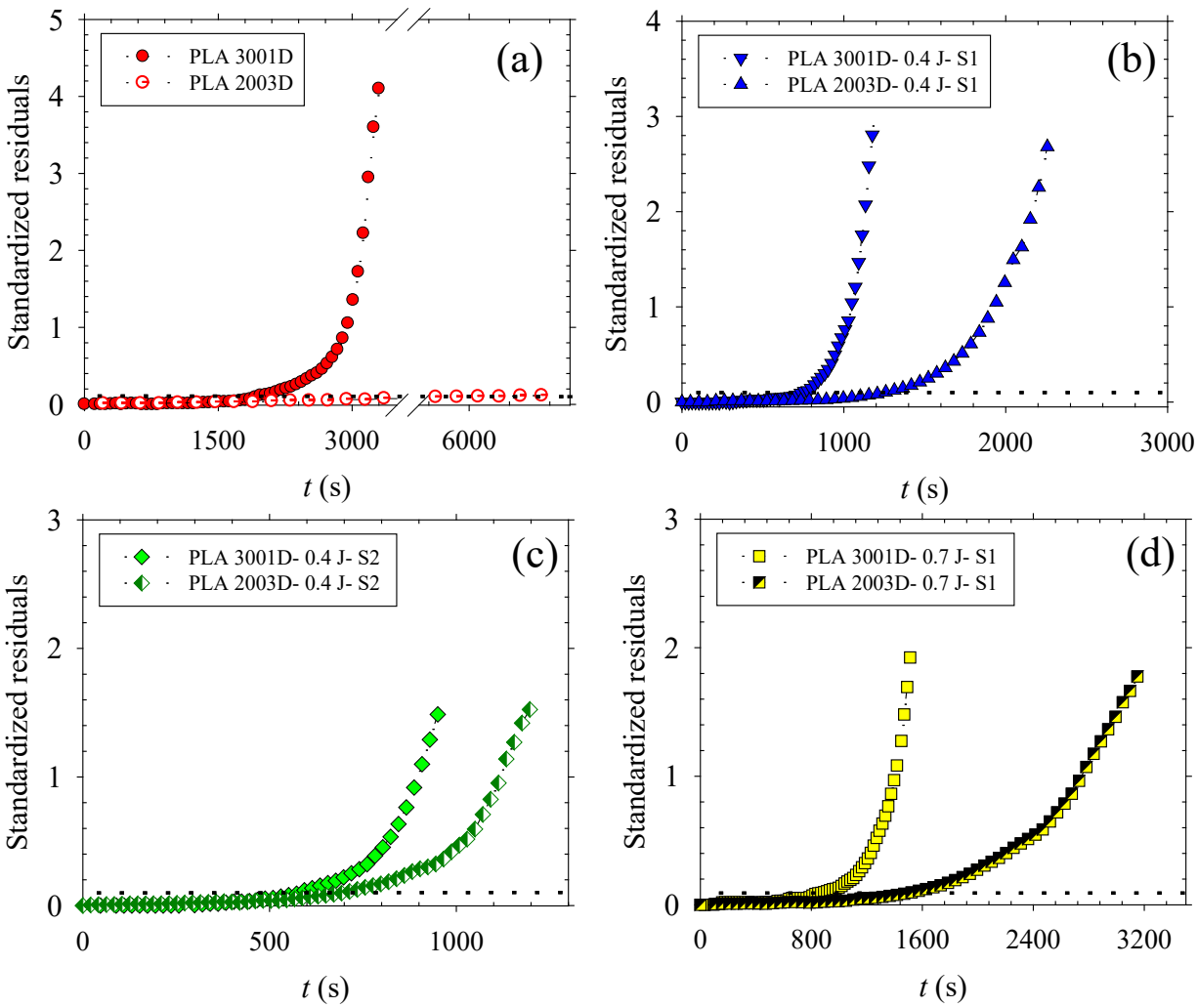

Fig. 6. Standardized residuals of the complex viscosity, η^*, for (a) the neat PLA 2003D, (b) PLA containing 0.4 wt% CE prepared using strategy S1, (c) PLA containing 0.4 wt% CE prepared using strategy S2 , and (d) PLA containing 0.7 wt% CE, as a function of time at 120 and 130 °C. The dash line shows the standardized residual value of 0.1.

The chain architecture is a critical parameter affecting the crystallization kinetics (Duplay et al. 1999; Heeley et al. 2006). The newly formed branched structure resulting from the addition of 0.4 wt% CE using strategy S1 leads to a significant reduction of the induction time, from above 6500 to 1250 s and from 1890 to 730 s for PLA 2003D and 3001D, respectively, at 130 °C (Fig. 6b). This time reduction suggests that the branched structure may accelerate the crystal nucleation by an heterogeneous mechanism (Yang et al. 2011), leading to an enhanced degree of crystallinity.

However, the branched structure may also increase the chain folding energy barrier and hinder PLA chains from folding back into crystal lamellae (Yu et al. 2009). For the case examined here, i.e. 0.4 wt% CE, the negative impact of branching on the crystallization kinetics seems overridden by the nucleation ability of the branches. The onset of crystallization of PLA 2003D and PLA 3001D is further reduced to 660 and 580 s, respectively, as LCB-PLA containing 0.4 wt% CE is produced using strategy S2 (Fig. 6c). The existence of highly branched macromolecules in comparison with sample S1 is responsible for the observed decrease of t_{in}.

Table 2. Induction time, t_{in}, for the onset of quiescent crystallization of the linear and LCB-PLAs prepared using two different grades and strategies at 130 °C. The experimental error is less than 8%.

Sample	t_{in} at 130 °C (s)	Sample	t_{in} at 130 °C (s)
PLA2003-Neat	-	PLA 3001-Neat	1890
PLA2003-0.4 J-S1	1250	PLA3001-0.4 J-S1	730
PLA2003-0.4 J-S2	660	PLA3001-0.4 J-S2	580
PLA2003-0.7 J- S1	1570	PLA 3001-0.7 J-S1	870

The higher degree of LCB due to the addition of 0.7 wt% CE increases the induction time of PLAs as shown in Fig. 6d and Table 2 (t_{in} of PLA2003D and PLA3001D increases from 660 to 1570 and from 580 to 870s, respectively). The observed increases of t_{in} may result from the detrimental impact of LCB on the chain folding energy barrier, as discussed earlier.This implies that there is a critical degree of LCB above which the effect is reversed

3-2. Shear-induced crystallization

In addition to the molecular structure, thermal history, and the presence of additives, flow conditions imposed on the polymer melt during processing are key factors influencing the crystallization kinetics. To investigate the impact of shear flow on the crystallization process, a

constant $\dot{\gamma}$ of 0.1 or 1 s^{-1} was applied to the different samples for 1, 5, and 10 min and, then, quenched from the initial flow temperature (180 °C) to the T_c (130 °C). To avoid repetition, focus is on PLA 3001D in this section since this sample is more prone to crystallization (lower *D*-content). The η_r^* values of the linear and LCB-PLAs prepared using different strategies are illustrated in Fig.7 as function of time. The corresponding induction times, t_{in}, are reported in Table 3. To further explore the effect of the applied shear rate on the crystallization process, the samples were pre-sheared at another constant rate, $\dot{\gamma}$, of 0.1 s^{-1} for 1, 5 and 10 min. The results are not presented here for the sake of brevity: however, the the measured t_{in} are provided in Table 3. Fig. 7a shows the η_r^* evolution of the linear PLA 3001D after different periods of shearing at a constant $\dot{\gamma}$ of 1 s^{-1}. The induction time for the onset of crystallization is reduced from 1810 to 1650 s, as reported in Table 3, for the sample subjected to 1 min pre-shearing (γ= 60). It is further decreased to 1390 and 1090 s as the pre-shearing time is increased to 5 min (γ= 300) and 10 min (γ= 600), respectively.

A reduction in the onset of crystallization as a consequence of increasing shear strain was also observed by other researchers in polybutene (Baert and Van Puyvelde 2006), polypropylene (PP) (Yu et al. 2009), and polycaprolactone (PCL) (Lellinger et al. 2003; Madbouly and Ougizawa 2003) systems. It is believed that the molecular chains are oriented and extended, and form "liquid fibrils" in the sheared melts (Lellinger et al. 2003; Yu et al. 2008). The pre-ordered chains or segments serve as precursors or primary nuclei for crystal nucleation, leading to an increase in the nucleation and crystallization growth rate (Lellinger et al. 2003; Madbouly and Ougizawa 2003; Yu et al. 2008). Once polymer melts are subjected to a longer pre-shearing time, more molecular chains are oriented and, thus, the crystal nucleation process is accelerated. A similar trend is observed in the crystallization behavior of the compounded samples S1 (Fig. 7b) and S2 (Fig. 7c),

and for the PLA containing 0.7 wt% CE (Fig. 7d). The results, furthermore, indicate that the impact of pre-shearing becomes more pronounced after the incorporation of CE into the PLA and the formation of an LCB structure. This pattern of behavior was also observed by Yu *et al* (Yu et al. 2009) for a LCB-PP system. The role of LCB and molecular weight on the shear-induced crystallization of PLA can be further clarified by defining a normalized induction time, $\theta = t_{in(s)}/t_{in(q)}$, as the ratio of the induction time at a given shear rate to the induction time under quiescent conditions.

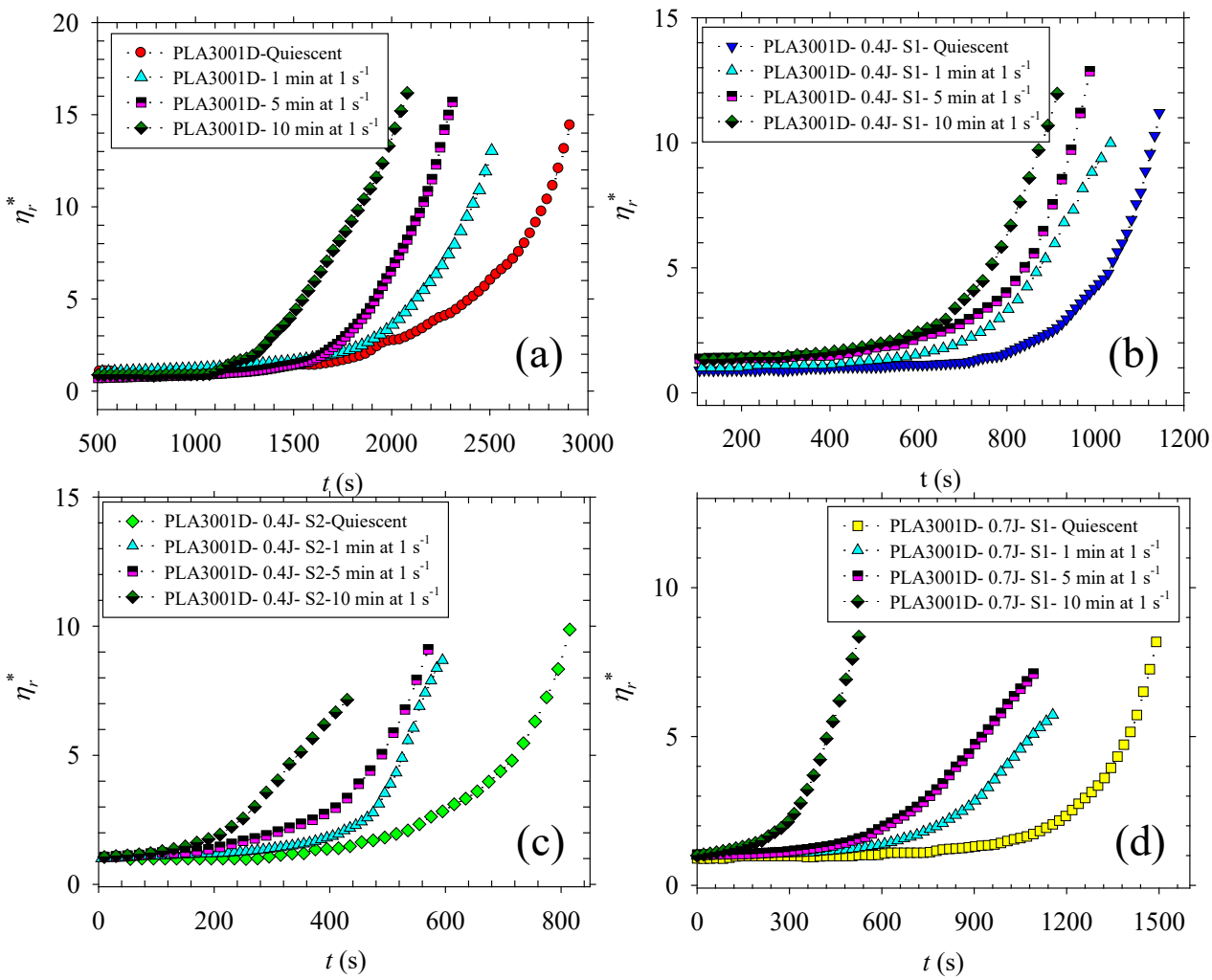

Fig. 7. Normalized complex viscosity, η_r^*, of (a) the neat PLA3001, PLA3001 containing 0.4 wt% CE prepared using (b) strategy S1, (c) strategy S2, and (d) PLA3001 containing 0.7 wt% CE, as a function of time after 1, 5, and 10 min preshearing at 1 s^{-1}: T_c = 130 °C.

Once polymer melts are subjected to a longer pre-shearing time, more molecular chains are oriented and, thus, the crystal nucleation process is accelerated. A similar trend is observed in the crystallization behavior of the compounded samples S1 (Fig. 7b) and S2 (Fig. 7c), and for the PLA containing 0.7 wt% CE (Fig. 7d). The results, furthermore, indicate that the impact of pre-shearing becomes more pronounced after the incorporation of CE into the PLA and the formation of an LCB structure. This pattern of behavior was also observed by Yu *et al* (Yu et al. 2009) for a LCB-PP system. The role of LCB and molecular weight on the shear-induced crystallization of PLA can be further clarified by defining a normalized induction time, $\theta = t_{in(s)}/t_{in(q)}$, as the ratio of the induction time at a given shear rate to the induction time under quiescent conditions.

Table 3. Induction time, t_{in} (s), for the onset of quiescent crystallization of the linear and LCB-PLAs after different periods of pre-shearing at $\dot{\gamma}$ of 0.1 and 1 s^{-1}. T_c was set at 130 °C and the experimental variability is less than 3%.

$\dot{\gamma}$ (s^{-1})	γ	PLA 3001-Neat	PLA3001-0.4 J-S1	PLA3001-0.4 J-S2	PLA 3001-0.7 J- S1	PLA 2003-0.4 J-S2	PLA 2003-0.7 J- S1
0.1	6	1840	695	545	775	-	-
0.1	30	1810	650	505	695	-	-
0.1	60	1745	590	460	645	550	1235
1	60	1725	580	445	625	-	-
1	300	1450	490	370	520	-	-
1	600	1140	375	195	220	440	750

The normalized induction time of the linear and LCB-PLAs prepared using different strategies after 1, 5 and 10 min pre-shearing is plotted as a function of shear rate, $\dot{\gamma}$, in Fig 8. The corresponding t_{in} for quiescent crystallization ($\dot{\gamma}$=0) is presented at $\dot{\gamma}$ of 10^{-3} s^{-1} instead of 0 for convenience. A comparison of Figs. 8a and b with Fig. 8c reveals that the normalized induction time, θ, of the linear and LCB-PLAs decreases with increasing pre-shearing time and shear rate.

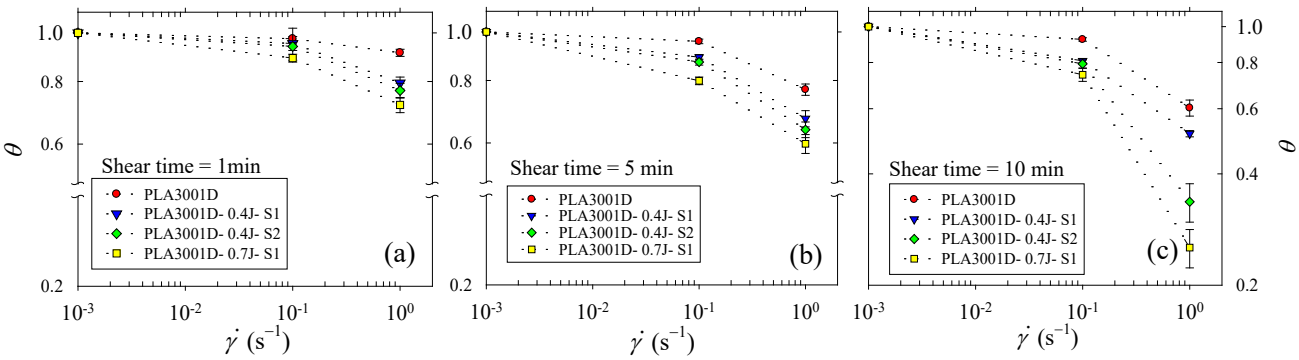

Fig. 8. Normalized induction time, $\theta = t_{in(s)}/t_{in(q)}$, of the linear and LCB-PLAs with various contents of CE prepared using different strategies as a function of shear rate after (a) 1 min, (b) 5 min and (c) 10 min preshearing. T_c was set at 130 °C. The PLA grade is 3001D.

For instance at $\dot{\gamma}$ of 1 s^{-1}, θ of the neat PLA3001D, S1 and S2 compounded samples, and PLA3001D containing 0.7 wt% CE drops from 0.77, 0.67, 0.64, and 0.60 to 0.61, 0.51, 0.34, and 0.25, respectively, as the pre-shearing time increases from 5 to 10 min. In addition, the normalized induction time drops more rapidly, particularly at $\dot{\gamma}$ of 1 s^{-1}, after the introduction of CE and increasing LCB structure. These results confirm that the LCB macromolecules play imperative key role on shear-induced crystallization. It has been generally accepted that the introduction of a LCB structure to the linear backbone of PLA leads to an increased M_w and, subsequently, to a larger relaxation time. The relaxation time spectra of these samples were calculated using the NLREG software (non-linear regularization) and presented in our previous work (Najafi et al. 2014). The characteristic relaxation time, λ_c, obtained for the linear PLA 3001D, S1, S2 compounded samples, and the PLA containing 0.7 wt% CE was 0.01, 0.76, 1.06, and 1.08 s, respectively. As discussed earlier, oriented nuclei will be formed under a shear flow. Once the deformation is withdrawn, they will relax to the original conformation, and therefore, crystallize quiescently. An increased relaxation time, resulting from the LCB structure, retards the relaxation process, which is favorable to retain the oriented chains and generate precursors of crystallization.

To evaluate how optical impurity (*D*-lactide content) influences the shear-induced crystallization behavior of PLA, LCB-PLAs based on PLA 2003D (containing 4.25 % *D*-lactide) were also subjected to 10 min pre-shearing at 0.1 and 1 s^{-1} and, then, the results compared with those obtained for PLA3001D (containing 1.5 % *D*-lactide). The θ values, of both PLA 2003D and 3001D, treated with 0.4 and 0.7 wt% CE after 10 min pre-shearing, are compared in Fig. 9 as a function of shear rate, $\dot{\gamma}$.

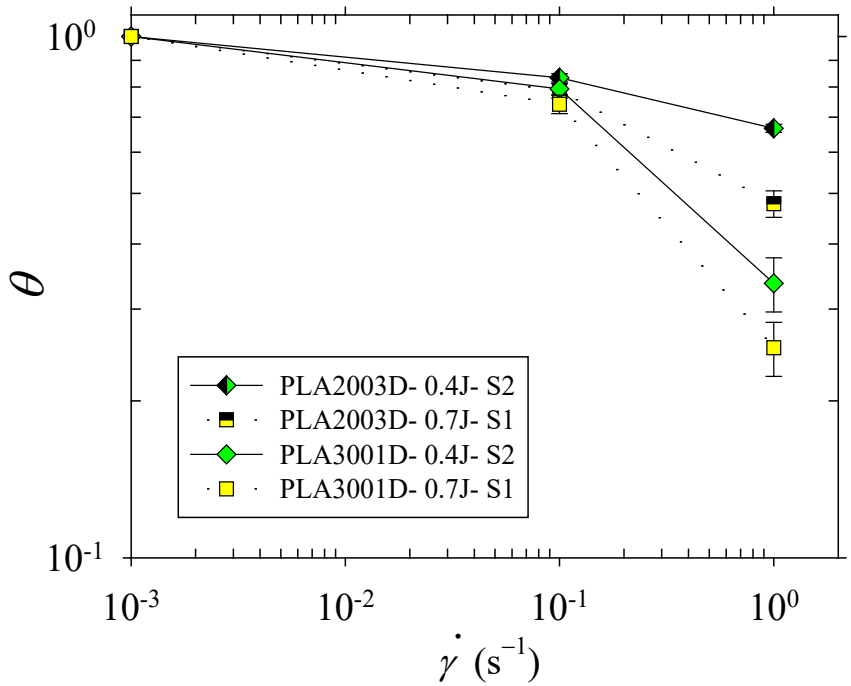

Fig. 9. Normalized induction time, θ, of PLA containing 0.4 and 0.7 wt % CE based on PLA 2003D and PLA 3001D, as a function of shear rate after 10 min pre-shearing. T_c was set at 130 °C. The error bars show the variation of the normalized induction time.

The θ values of the LCB-PLAs based on PLA 2003D are less reduced with increasing shear rate in comparison with the corresponding values of samples based on PLA 3001D. For example, θ of the PLA2003D treated with 0.4 and 0.7 wt% CE decreases to 0.79 and 0.48, respectively, after 10 min pre-shearing at 1 s^{-1}, indicating that PLA 2003D is less sensitive than PLA 3001D to the applied

shear due to its lower ability to crystallize. The optically impure *D*-lactide units are found to incorporate defects into the crystal structure, leading to a delayed crystal nucleation and decelerated growth rate (Tsuji and Ikada 1996; Baratian et al. 2001). In addition to total strain, γ, the contribution of the shear rate, $\dot{\gamma}$, to the crystallization kinetics was investigated at three different values, 0.5, 0.8, and 1 s^{-1}, for a constant γ of 300. Two different compositions were considered in this part of the study; the linear PLA3001D with the longest induction time in quiescent conditions (1890 s) and the PLA3001D treated with 0.4 wt% of CE prepared using strategy S2 with the shortest induction time (580 s).

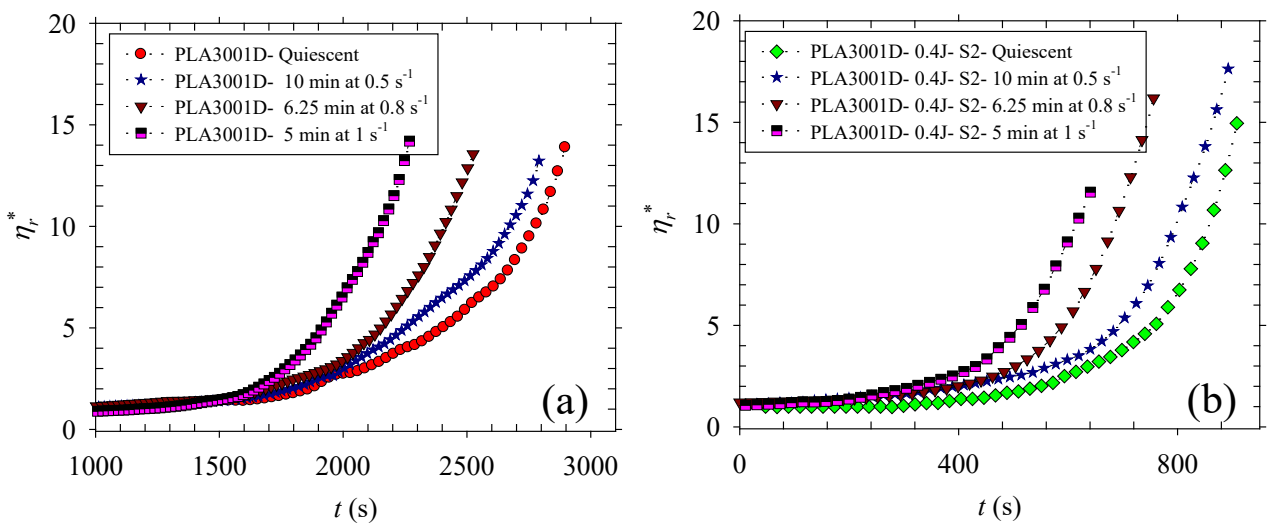

Fig. 10. Normalized complex viscosity, η_r^*, of (a) the neat PLA 3001D, (b) PLA containing 0.4 wt% CE prepared using strategy S2 as a function of time after preshearing at shear rate, $\dot{\gamma}$, of 0.5, 0.8 and 1 s^{-1} while keeping constant the total strain (γ = 300). T_c was set at 130 °C.

The results for the η_r^* evolution are presented in Fig. 10. The corresponding induction times were obtained with an experimental error of less than 5 %, and are reported in Table 4. As the shear rate is increased from 0.5 to 0.8 s^{-1}, t_{in} is reduced from 1740 to 1575s for the linear PLA, and from 515 to 460 s for the LCB-PLA. With increasing $\dot{\gamma}$ to 1 s^{-1}, t_{in} of the linear and LCB-PLAs is further decreased to 1450 and 370 s, respectively.

Table 4. Induction time, t_{in} (s), for the onset of crystallization for the linear and LCB-PLA (3001D) after pre-shearing at $\dot{\gamma}$ of 0.5, 0.8, and 1 s^{-1}, while keeping the total strain, γ, equal to 300. T_c was set at 130 °C and the experimental variability was less than 5%.

Shear time (s)	$\dot{\gamma}$ (s^{-1})	γ	Neat PLA 3001	PLA3001-0.4 J-S2
Quiescent	0	0	1890	580
600	0.5	300	1740	515
375	0.8	300	1575	460
300	1	300	1450	370

This result implies that a higher shear rate applied for a shorter time is more effective to initiate crystallization than a lower shear rate for a longer time. A similar observation was also reported in the literature (Baert and Van Puyvelde 2006; Yu et al. 2008) for other polymeric materials.

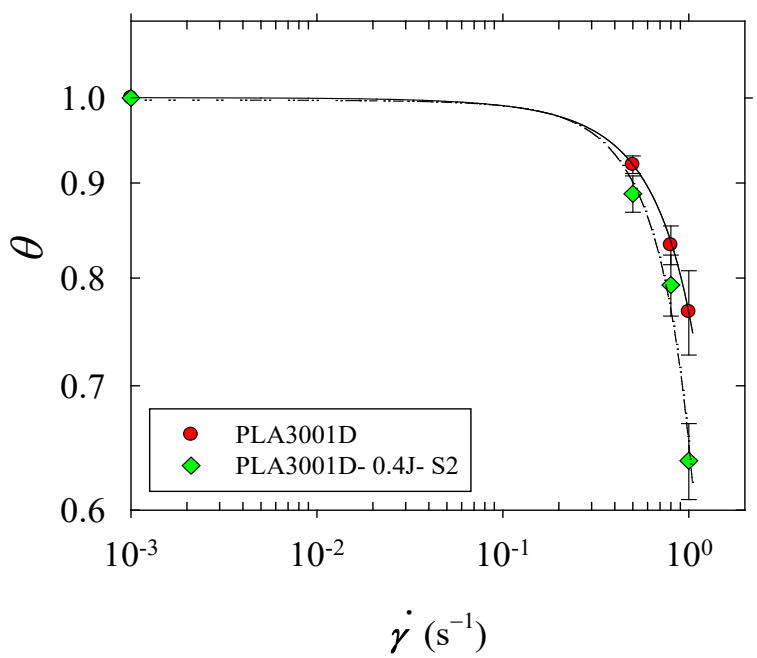

Fig. 11. Normalized induction time, θ, of the neat PLA3001D and PLA3001D treated with 0.4 wt% CE prepared using strategy S2 after pre-shearing at $\dot{\gamma}$ of 0.5, 0.8, and 1 s^{-1} while keeping the total strain, γ, equal to 300. T_c was set at 130 °C.

The observed phenomenon, indeed, results from the impact of shear rate on the degree of orientation in the molecular chains. As the shear rate is decreased, even at large shear strain, the

molecular chains have more time for relaxing back to their original conformation. Consequently, less oriented chain segments are formed to promote nucleation and reduce the induction time.

It is worth to note that the sensitivity of the normalized induction time to the applied $\dot{\gamma}$, illustrated in Fig. 11 at a constant total strain (γ = 300), is more evident after the incorporation of the LCB structure into PLA and increased M_w.

3-3. Morphology

To assess how the LCB structure and pre-shearing influence the crystallization, the morphology of the linear PLA (PLA 3001D) and the LCB-PLA (PLA 3001D treated with 0.4 wt % CE and prepared using strategy S2) was monitored using the Linkam optical shearing system. The isothermal crystallization of the linear and LCB-PLAs was conducted at 130 °C under quiescent conditions and after 5 min pre-shearing at $\dot{\gamma}$ of 1 s^{-1}. The results for the crystal structure development of the linear and LCB- PLAs under quiescent conditions and after a step shear are presented in Fig. 12. The spherulite density of these samples, evaluated from optical photomicrographs after 8 min of annealing, is given in Table 5.

Table 5. The spherulite density of the linear and LCB-PLA (3001D) at quiescent and after 300 s pre-shearing at rate of 1 s^{-1}. The crystallization temperature was set at 130 °C.

Shear time (s)	$\dot{\gamma}$ (s^{-1})	γ	Neat PLA 3001	PLA3001-0.4 J-S2
			Spherulite density, #/mm^2	Spherulite density, #/mm^2
Quiescent	0	0	1050	7000
300	1	300	1400	8050

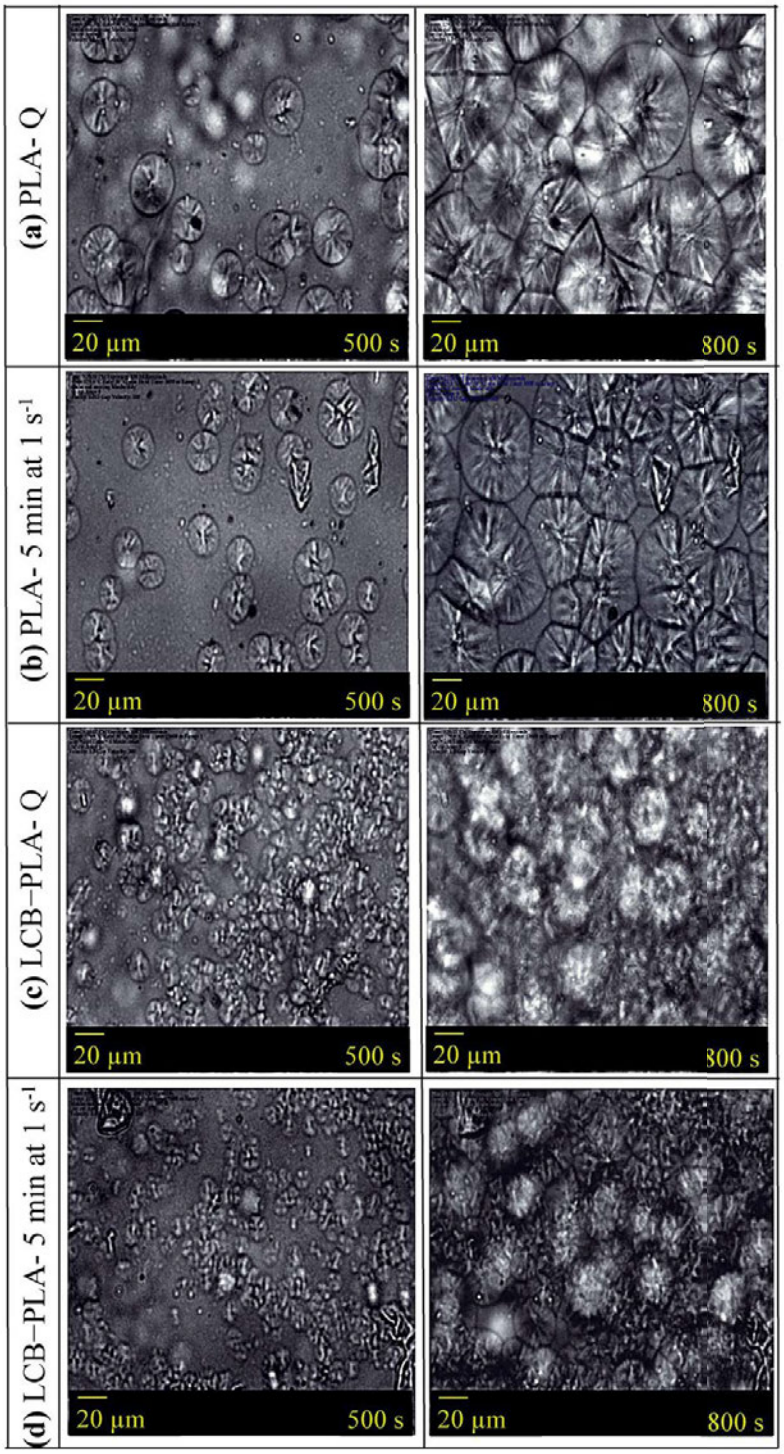

Fig. 12. Characteristic crystal morphologies of (a) the linear PLA3001D in quiescent conditions, (b) linear PLA subjected to 5 min pre-shearing at $\dot{\gamma}$ of 1 s^{-1}, (c) LCB-PLA3001D in quiescent conditions, (d) LCB-PLA subjected to 5 min pre-shearing at $\dot{\gamma}$ of 1 s^{-1}. LCB-PLA3001D was produced by incorporating 0.4 wt% CE using strategy S2. Tests were performed at 130 ^{o}C after 500 and 800 s annealing times.

The linear PLA (Fig. 12a) exhibits a well-defined spherulitic structure. The crystals grow and impinge upon each other as the annealing time increases. The variation of the size of the spherulites with time reflects the crystallization kinetics of the polymer and the average radius size of unimpinged spherulite measured as a function of time is reported in Fig. 13.

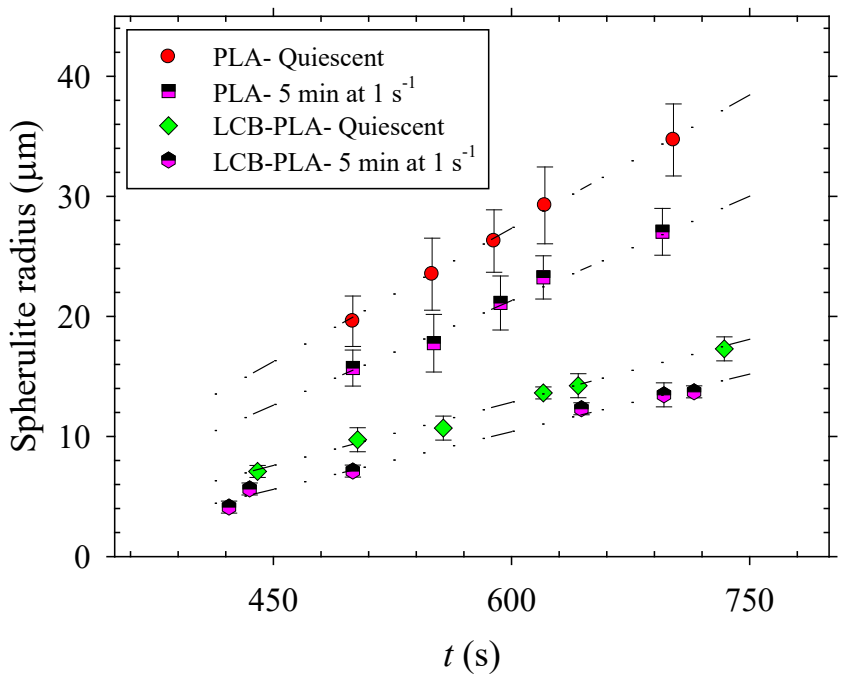

Fig. 13. Average radius of unimpinged spherulites for the linear and LCB-PLA3001Ds under isothermal crystallization as a function of time. T_c was set at 130 °C.

The crystal size is found to increase linearly with time. As seen in Table 5, the number of spherulites after 8 min annealing is increased from 1050 crystals/mm^2 under quiescent conditions to 1400 crystals/mm^2 after imposing a shear flow (5 min at $\dot{\gamma}$ of 1 s^{-1}) on the polymer melt; an increment in the number of spherulites limits their growth, resulting in a smaller crystal size as shown in Figs. 12b and 13. These findings are in good agreement with the results reported by (Favaro et al. 2009) and (Baert and Van Puyvelde 2006) for different polymeric materials. Fig. 12c displays the crystal morphology and size of LCB-PLA under quiescent conditions for two different

annealing times. In comparison with the linear PLA (Fig. 12a), the number of spherulites is impressively increased (from 1050 to 7000 crystals/ mm^2) while the average crystal size also drops considerably (Fig. 13). This evidence confirms that the LCB structure acts as nucleation sites and enhances the crystallinity of PLA. Based on the results presented in Fig. 13, the radial growth rate of spherulites reduces from 4.4 μm/min for the neat PLA to 2.0 μm/min after the introduction of the LCB structure in quiescent conditions. This reduction was also observed by (Liu et al. 2012), and is mainly attributed to the dramatic increase in the spherulite density, which limits the growth rate of the crystallites. Fig. 12d shows the impact of pre-shearing on the crystal morphology of LCB-PLA. Similar to what was observed for the linear counterpart, the number of spherulites is further increased from 7000 to 8050 crystals/mm^2, and the size of crystal slightly decreases (see Fig. 13) as a shear field is applied. An increase of the spherulite density under shear induced conditions leads to reduction of the spherulite growth rate when compared with results in quiescent conditions. The spherulite growth rate of the neat PLA and LCB structure is respectively reduced from 4.4 to 3.5 and from 2.0 to1.8 μm/min under shear induced conditions. . Considering that the impact of the applied shear on increasing the spherulite density of the neat PLA (33 %) is more pronounced than for the LCB-PLA (15 %), a further reduction in its growth rate is expected.

It is of interest to compare the structure development observed by optical microscopy with the evolution of the storage modulus, η_r^*, obtained in rheological measurements. Similar to the study reported for PCL (Acierno et al. 2006), the spherulites are found to appear and grow when η_r^* is still constant in the plateau region. In fact, the structure development can be detected by microscopy and consists of small spherulites surrounded by the amorphous matrix phase, even within the onset time determined by rheometry. Such a behavior was also observed by other authors (Bove and Nobile 2002; Hadinata et al. 2005; R. Iervolino 2006) for polybutene (PB).

Considering that the crystallization is a local phenomenon and the rheometer measures an overall macroscopic viscosity of the melt, a recently developed device, called RheoDSC (Kiewiet et al. 2008), is suggested for these types of experiments. This technique allows a simultaneous combination of in situ rheological measurements and thermal analysis (DSC) on the same sample.

Conclusion

The isothermal crystallization behavior of linear and long-chain branched (LCB) PLAs, based on two different grades of PLA, 3001D and 2003D, was investigated under quiescent and shear flow conditions using rheometry and optical microscopy. LCB-PLAs were prepared by a melt grafting reaction in the presence of a multi-functional chain extender (CE). The quiescent crystallization behavior of the linear and LCB structures of both PLA grades was studied at 130 ^{o}C. In comparison with the PLA 2003D, PLA 3001D exhibited a shortened crystallization induction time due to its lower *D*-lactide content. The incorporation of an LCB structure into linear PLA using 0.4 wt % CE promoted the crystallization kinetics, thus leading to shorter induction times. The impact of shear on the crystallization of PLA was also examined. The shear-induced crystallization of the linear and LCB-PLAs was influenced not only by the total shear strain but also by the shear rate. To determine the effect of shear strain, a pre-shear treatment was applied on the melt at constant shear rates of 0.1 and 1 s^{-1} for a period of 1, 5, and 10 min. The obtained results implied that increase of total shear strain further decreased the onset time of crystallization. The shear strain impact on the crystallization kinetics was more pronounced as the degree of LCB and molecular weight increased. To assess the role of shear rate on the induced crystallization, pre-shear was applied at rates of 0.5, 0.8, and 1 s^{-1} while keeping the total strain constant (γ=300). The induction

time of linear and LCB-PLAs was shortened as the shear rate increased for the same total shear strain.

The crystal morphology of the linear and LCB- PLAs under quiescent and shear flow conditions was observed using a Linkam optical shear system. The optical micrographs provided information about the spherulite density and growth rate. An increase in the spherulite density was observed in the strained melt of both linear and LCB-PLAs, as compared with those of unstrained counterparts. A comparison of the crystal structure of linear PLA with that of LCB-PLA revealed that long chain branching significantly promoted the nucleation density, although it diminished the crystal growth rate (from 4.4 to 2 μm/min for neat PLA).

Acknowledgements

Financial support from Auto 21 (Canada's automotive R&D program) and NCE (Networks of Centres of Excellence of Canada) is gratefully acknowledged.

References

Achmad F, Yamane K, Quan S, Kokugan T (2009) Synthesis of polylactic acid by direct polycondensation under vacuum without catalysts, solvents and initiators Chemical Engineering Journal 151:342-350 doi:http://dx.doi.org/10.1016/j.cej.2009.04.014

Acierno S, Di Maio E, Iannace S, Grizzuti N (2006) Structure development during crystallization of polycaprolactone Rheol Acta 45:387-392 doi:10.1007/s00397-005-0054-2

Acierno S, Palomba B, Winter H, Grizzuti N (2003) Effect of molecular weight on the flow-induced crystallization of isotactic poly(1-butene) Rheol Acta 42:243-250 doi:10.1007/s00397-002-0280-9

Ahn SH, Cho CB, Lee KY (2002) The Kinetics of Shear-Induced Crystallization in Poly(Ethylene Terephthalate) Journal of Reinforced Plastics and Composites 21:617-628 doi:10.1177/0731684402021007026

Arias A (2014) Development of Natural Fiber Reinforced Polylactide-Based Biocomposites. Dissertation, Ecole Polytechnique of Montreal

Arias A, Heuzey M-C, Huneault M (2013) Thermomechanical and crystallization behavior of polylactide-based flax fiber biocomposites Cellulose 20:439-452 doi:10.1007/s10570-012-9836-8

Baert J, Van Puyvelde P (2006) Effect of molecular and processing parameters on the flow-induced crystallization of poly-1-butene. Part 1: Kinetics and morphology Polymer 47:5871-5879 doi:http://dx.doi.org/10.1016/j.polymer.2006.06.009

Baratian S, Hall ES, Lin JS, Xu R, Runt J (2001) Crystallization and Solid-State Structure of Random Polylactide Copolymers: Poly(l-lactide-co-d-lactide)s Macromolecules 34:4857-4864 doi:10.1021/ma001125r

Bove L, Nobile MR (2002) Shear-induced crystallization of isotactic poly(1-butene) Macromolecular Symposia 185:135-147 doi:10.1002/1521-3900(200208)185:1<135::aid-masy135>3.0.co;2-s

Chen Q, Fan Y-r, Zheng Q (2007) Shear induced crystallization of high-density polyethylene Journal of Central South University of Technology 14:174-177 doi:10.1007/s11771-007-0239-1

Drumright RE, Gruber PR, Henton DE (2000) Polylactic Acid Technology Advanced Materials 12:1841-1846 doi:10.1002/1521-4095(200012)12:23<1841

Duplay C, Monasse B, Haudin J-M, Costa J-L (1999) Shear-induced crystallization of polypropylene: influence of molecular structure Polymer International 48:320-326 doi:10.1002/(sici)1097-0126(199904)48:4<320::aid-pi164>3.0.co;2-7

Eslami H, Kamal MR (2013) Effect of a chain extender on the rheological and mechanical properties of biodegradable poly(lactic acid)/poly[(butylene succinate)-co-adipate] blends Journal of Applied Polymer Science 129:2418-2428 doi:10.1002/app.38449

Favaro MM, Rego BT, Branciforti MC, Bretas RES (2009) Study of the quiescent and shear-induced crystallization kinetics of intercalated PTT/MMT nanocomposites Journal of Polymer Science Part B: Polymer Physics 48:113-127 doi:10.1002/polb.21852

Garlotta D (2001) A literature review of poly(lactic acid) Journal of Polymers and the Environment 9:63-84 doi:Unsp 1566-2543/01/0400-0063/0

Haas TW, Maxwell B (1969) Effects of shear stress on the crystallization of linear polyethylene and polybutene-1 Polymer Engineering & Science 9:225-241 doi:10.1002/pen.760090402

Hadinata C, Gabriel C, Ruellman M, Laun HM (2005) Comparison of shear-induced crystallization behavior of PB-1 samples with different molecular weight distribution Journal of Rheology (1978-present) 49:327-349 doi:doi:http://dx.doi.org/10.1122/1.1835342

Han L, Han C, Dong L (2013) Effect of crystallization on microstructure and mechanical properties of poly[(ethylene oxide)-block-(amide-12)]-toughened poly(lactic acid) blend Polymer International 62:295-303 doi:10.1002/pi.4300

Heeley EL et al. (2006) Shear-Induced Crystallization in Blends of Model Linear and Long-Chain Branched Hydrogenated Polybutadienes Macromolecules 39:5058-5071 doi:10.1021/ma0606307

Hu W (2001) Chain folding in polymer melt crystallization studied by dynamic Monte Carlo simulations The Journal of Chemical Physics 115:4395-4401 doi:doi:http://dx.doi.org/10.1063/1.1389860

Jabbarzadeh A, Tanner RI (2010) Flow-Induced Crystallization: Unravelling the Effects of Shear Rate and Strain Macromolecules 43:8136-8142 doi:10.1021/ma100985x

Kausch H-H, Chan C-M, Li L (2005) Direct Observation of the Growth of Lamellae and Spherulites by AFM. In: Intrinsic Molecular Mobility and Toughness of Polymers II, vol 188. Advances in Polymer Science. Springer Berlin Heidelberg, pp 1-41. doi:10.1007/b136971

Kiewiet S, Janssens V, Miltner HE, Van Assche G, Van Puyvelde P, Van Mele B (2008) RheoDSC: A hyphenated technique for the simultaneous measurement of calorimetric and rheological evolutions Review of Scientific Instruments 79:- doi:doi:http://dx.doi.org/10.1063/1.2838585

Kim SH, Han Y-K, Kim YH, Hong SI (1992) Multifunctional initiation of lactide polymerization by stannous octoate/pentaerythritol Die Makromolekulare Chemie 193:1623-1631 doi:10.1002/macp.1992.021930706

Kramschuster A, Turng L-S (2009) An injection molding process for manufacturing highly porous and interconnected biodegradable polymer matrices for use as tissue engineering scaffolds Journal of Biomedical Materials Research Part B: Applied Biomaterials 92B:366-376 doi:10.1002/jbm.b.31523

Lellinger D, Floudas G, Alig I (2003) Shear induced crystallization in poly(Îµ-caprolactone): effect of shear rate Polymer 44:5759-5769 doi:http://dx.doi.org/10.1016/S0032-3861(03)00633-5

Li L, Chan C-M, Yeung KL, Li J-X, Ng K-M, Lei Y (2000) Direct Observation of Growth of Lamellae and Spherulites of a Semicrystalline Polymer by AFM Macromolecules 34:316-325 doi:10.1021/ma000273e

Liedauer S, Eder G, Janeschitz-Kriegl H, Jerschow P, Geymayer W, Ingolic E (1993) On the Kinetics of Shear Induced Crystallization in Polypropylene International Polymer Processing 8:236-244 doi:10.3139/217.930236

Liu J, Zhang S, Zhang L, Bai Y (2012) Crystallization Behavior of Long-Chain Branching Polylactide Industrial & Engineering Chemistry Research 51:13670-13679 doi:10.1021/ie301567n

Lunt J (1998) Large-scale production, properties and commercial applications of polylactic acid polymers Polymer Degradation and Stability 59:145-152 doi:http://dx.doi.org/10.1016/S0141-3910(97)00148-1

Ma Z, Balzano L, van Erp T, Portale G, Peters GWM (2013) Short-Term Flow Induced Crystallization in Isotactic Polypropylene: How Short Is Short? Macromolecules 46:9249-9258 doi:10.1021/ma401833k

Madbouly SA, Ougizawa T (2003) Rheological Investigation of Shear-Induced Crystallization of Poly(Ïµ-Caprolactone) Journal of Macromolecular Science, Part B 42:269-281 doi:10.1081/mb-120017118

Meng Q, Heuzey M-C, Carreau PJ (2012) Control of thermal degradation of polylactide/clay nanocomposites during melt processing by chain extension reaction Polymer Degradation and Stability 97:2010-2020 doi:http://dx.doi.org/10.1016/j.polymdegradstab.2012.01.030

Mujica-Garcia A, Navarro-Baena I, Kenny JM, Peponi L (2014) Influence of the Processing Parameters on the Electrospinning of Biopolymeric Fibers Journal of Renewable Materials doi:10.7569/jrm.2013.634130

Nagahata R, Sano D, Suzuki H, Takeuchi K (2007) Microwave-Assisted Single-Step Synthesis of Poly(lactic acid) by Direct Polycondensation of Lactic Acid Macromolecular Rapid Communications 28:437-442 doi:10.1002/marc.200600715

Najafi N, Heuzey M-C, Carreau P, Therriault D, Park C (2014) Rheological and foaming behavior of linear and branched polylactides Rheol Acta 53:779-790 doi:10.1007/s00397-014-0801-3

Najafi N, Heuzey MC, Carreau PJ (2013) Crystallization behavior and morphology of polylactide and PLA/clay nanocomposites in the presence of chain extenders Polymer Engineering & Science 53:1053-1064 doi:10.1002/pen.23355

Najafi N, Heuzey MC, Carreau PJ, Wood-Adams PM (2012) Control of thermal degradation of polylactide (PLA)-clay nanocomposites using chain extenders Polymer Degradation and Stability 97:554-565 doi:http://dx.doi.org/10.1016/j.polymdegradstab.2012.01.016

R. Iervolino (2006) Rheology and morphology of the flow induced crystallization in polymers. University of Salerno

Ryan Anthony J, Terrill Nicholas J, Fairclough JPA (1999) A Scattering Study of Nucleation Phenomena in Homopolymer Melts. In: Scattering from Polymers, vol 739. ACS Symposium Series. American Chemical Society, pp 201-217. doi:doi:10.1021/bk-2000-0739.ch013

Suryanegara L, Nakagaito AN, Yano H (2009) The effect of crystallization of PLA on the thermal and mechanical properties of microfibrillated cellulose-reinforced PLA composites Composites Science and Technology 69:1187-1192 doi:http://dx.doi.org/10.1016/j.compscitech.2009.02.022

Tsuji H, Ikada Y (1996) Crystallization from the melt of poly(lactide)s with different optical purities and their blends Macromolecular Chemistry and Physics 197:3483-3499 doi:10.1002/macp.1996.021971033

Wang L, Jing X, Cheng H, Hu X, Yang L, Huang Y (2012a) Blends of Linear and Long-Chain Branched Poly(l-lactide)s with High Melt Strength and Fast Crystallization Rate Industrial & Engineering Chemistry Research 51:10088-10099 doi:10.1021/ie300526u

Wang L, Jing X, Cheng H, Hu X, Yang L, Huang Y (2012b) Rheology and Crystallization of Long-Chain Branched Poly(l-lactide)s with Controlled Branch Length Industrial & Engineering Chemistry Research 51:10731-10741 doi:10.1021/ie300524j

Wang Z-Y, Li X-W, Li J-N, Li G-M, Tao J-Q (2009) Synthesis of poly(lactic acid)-poly(phenyl phosphate) via direct polycondensation and its characterization Journal of Polymer Research 16:255-261 doi:10.1007/s10965-008-9224-0

Wereta A, Gogos CG (1971) Crystallization studies on deformed polybutene-1 melts Polymer Engineering & Science 11:19-27 doi:10.1002/pen.760110105

Yang B, Yang M, Wang W-J, Zhu S (2011) Effect of long chain branching on nonisothermal crystallization behavior of polyethylenes synthesized with constrained geometry catalyst Polymer Engineering & Science 52:21-34 doi:10.1002/pen.22040

Yu F, Zhang H, Liao R, Zheng H, Yu W, Zhou C (2009) Flow induced crystallization of long chain branched polypropylenes under weak shear flow European Polymer Journal 45:2110-2118 doi:http://dx.doi.org/10.1016/j.eurpolymj.2009.03.011

Yu F, Zhang H, Zheng H, Yu W, Zhou C (2008) Experimental study of flow-induced crystallization in the blends of isotactic polypropylene and poly(ethylene-co-octene) European Polymer Journal 44:79-86 doi:http://dx.doi.org/10.1016/j.eurpolymj.2007.10.022

Yuryev Y, Wood-Adams P (2010) Rheological properties of crystallizing polylactide: Detection of induction time and modeling the evolving structure and properties Journal of Polymer Science Part B: Polymer Physics 48:812-822 doi:10.1002/polb.21953